Journal of Materials Chemistry A

ROYAL SOCIETY OF CHEMISTRY

PAPER

View Article Online
View Journal | View Issue

Cite this: J. Mater. Chem. A, 2022, 10, 1343

Reducing sputter induced stress and damage for efficient perovskite/silicon tandem solar cells†

Kong Liu, [ab] Bo Chen,*[bc] Zhengshan J. Yu,[d] Yulin Wu,[a] Zhitao Huang,[a] Xiaohao Jia,[a] Chao Li,[a] Derrek Spronk,[c] Zhijie Wang,[a] Zhanguo Wang,[a] Shengchun Qu,*[a] Zachary C. Holman*[d] and Jinsong Huang*[bc]

Received 24th October 2021
Accepted 10th December 2021

DOI: 10.1039/d1ta09143c

rsc.li/materials-a

Reducing damage caused by sputtering of transparent conductive oxide (TCO) electrodes is critical in achieving highly efficient and stable perovskite/silicon tandem solar cells. Here we study the sputter caused damage to bathocuproine (BCP), which is widely used in highly efficient p–i–n structure single junction perovskite solar cells. While the BCP buffer layer protects the underlying layers from damage, it itself can be damaged by sputtering of TCOs at a wide range of target–substrate distances, supported by molecular dynamics simulation. More intriguingly, it is observed that TCO easily peeled off after sputtering when the sputtering target is close to the substrate. This is ascribed to the formation of stress during the cooling down process after sputtering due to different thermal expansion coefficients of the layers. Our studies explain why tin oxide (SnO_2) made by atomic layer deposition can replace BCP for a much better tandem device performance. SnO_2 has high affinity with the sputtered TCO electrode to suppress the peeling-off issue and has higher bond energy to resist sputter induced damage, thus allowing a wider window of target–substrate distances than BCP during TCO sputtering. Ultimately, we demonstrate an efficient perovskite/silicon monolithic tandem solar cell with an efficiency of 26.0% to illustrate the beneficial effects of reduced stress and damage.

1 Introduction

Metal halide perovskite/silicon tandem solar cells are promising for achieving efficiency beyond that of single-junction solar cells, potentially resulting in lower levelized cost of electricity.[1–9] In these solar cells, transparent conductive electrodes are required to transmit the incident sunlight. Transparent conductive oxides (TCO) such as indium zinc oxide (IZO) have been widely used as top electrodes in semitransparent solar cells and tandem solar cells.[10–13] Magnetron sputtering is the most widely used industrial technique to deposit IZO.[14] However, some challenges may arise when IZO sputtering is applied to perovskite top sub-cells. The first one is that the mismatch of thermal expansion coefficients between layers may introduce stress in films, since the sputtering process could involve a large temperature change. The second is that high-energy sputtered atoms, ions, electrons, or ultraviolet light produced during sputtering processes may damage the perovskite or organic layers in perovskite solar cells by changing their chemical bonding.[15,16]

The typical single-junction p–i–n structure perovskite solar cells have a structure of ITO/poly(triaryl amine)/perovskite/ETL/BCP/Cu, where ETL is the electron transport layer such as phenyl-C61-butyric acid methyl ester, Indene C_{60} Bis Adduct (ICBA), C_{60}, or a double fullerene layer.[17,18] The BCP buffer layer is very important for high-performance solar cells, because it reduces charge recombination at the ETL/Cu interface.[19–21] But, as a soft organic material, BCP suffers from damage when the thermally evaporated Cu electrode is replaced with sputtered TCO. Several studies employed perovskite top cells with SnO_2, which is deposited by atomic layer deposition (ALD), as the buffer layer to reduce sputter damage during TCO deposition.[22–25] However, there is no study yet about the stress in the sputtered IZO electrode and corresponding peeling-off issue when the stress is out of the tolerance range. It is yet unclear how the sputtering process actually damages BCP, and why SnO_2 can resist the damage. It is also unknown whether the sputtering process would damage layers underneath BCP, such as C_{60} and perovskite films. Moreover, whether SnO_2 can tolerate the sputter induced stress and avoid sputter damage under any sputtering condition needs to be investigated as well. Clarifying these issues will help us to determine sputtering

[a]Key Laboratory of Semiconductor Materials Science, Institute of Semiconductors, Chinese Academy of Sciences, Beijing, 100083, China. E-mail: qsc@semi.ac.cn
[b]Department of Mechanical and Materials Engineering, University of Nebraska-Lincoln, Lincoln, NE 68588, USA
[c]Department of Applied Physical Sciences, University of North Carolina, Chapel Hill, NC 27599, USA. E-mail: jhuang@unc.edu; bochen@unc.edu
[d]School of Electrical, Computer, and Energy Engineering, Arizona State University, Tempe, AZ 85287, USA. E-mail: Zachary.Holman@asu.edu

† Electronic supplementary information (ESI) available. See DOI: 10.1039/d1ta09143c

parameters for TCO of perovskite/silicon tandem solar cells, which is vital for balance between the fabrication cost and materials properties.

In this work, we investigate the stress related damage issue induced by sputtering IZO when different buffer layers of BCP and SnO_2 are used. We present mechanisms and mitigation approaches for sputter induced stress in perovskite solar cells. The reasons for better performance in the semi-transparent solar cells with the SnO_2 buffer layer than that with the BCP buffer layer are discussed. Molecular dynamics (MD) simulations are introduced to understand the damage process of sputtered atoms on BCP. Also, the possible peeling-off risk in the IZO electrode on the SnO_2 buffer layer is examined, and the method to overcome it is provided. An efficient perovskite/silicon tandem solar cell is presented to prove the beneficial effect of our strategies.

2 Results and discussion

2.1 Peeling-off phenomenon in IZO

We first observed the peeling-off problem of the sputtered IZO electrode for semitransparent perovskite solar cells with BCP and SnO_2 buffer layers. The main parameter we tuned in this study was the target–substrate distance, as illustrated in Fig. 1a. Peeling-off of the IZO electrode from underlying layers after sputtering on semitransparent perovskite solar cells with the BCP buffer layer was observed at a wide range of target–substrate distances from 8 cm to 12 cm; while this peeling-off issue only happened at a short target–substrate distance of 8 cm for solar cells with the SnO_2 buffer layer, as shown in Fig. 1b and S1.† It was noted that the peeling-off phenomenon didn't occur during the sputtering process but occurred after sputtering during the sample cooling down process, which indicates that the change of thermal conditions may be the reason for the phenomenon. The cross-sectional SEM image in Fig. 1c shows that the peeling-off issue caused bad contact between the IZO electrode and underlying layer.

2.2 Mechanism for sputter induced stress reduction

The peeling-off phenomenon of the IZO electrode indicates that there is stress in the sputtered IZO electrode. We speculated that a mismatch of the thermal expansion coefficients between the sputtered IZO layer and the underlying layers caused the peeling-off issue. To test this hypothesis, we measured the temperature of the sample surface during sputtering at different target–substrate distances with temperature indicators. This experiment revealed that the temperature reached 71 °C, 54 °C and 43 °C when the substrate–target distances were 8 cm, 10 cm and 12 cm, respectively, but the temperature remained below 37 °C when the substrate–target distance increased to 14 cm. It has been reported that the kinetic energy of sputtered atoms can reach 100 eV, which is about 100 times larger than the energies of evaporated particles.[26,27] This kinetic energy can convert to thermal energy after bombardment with

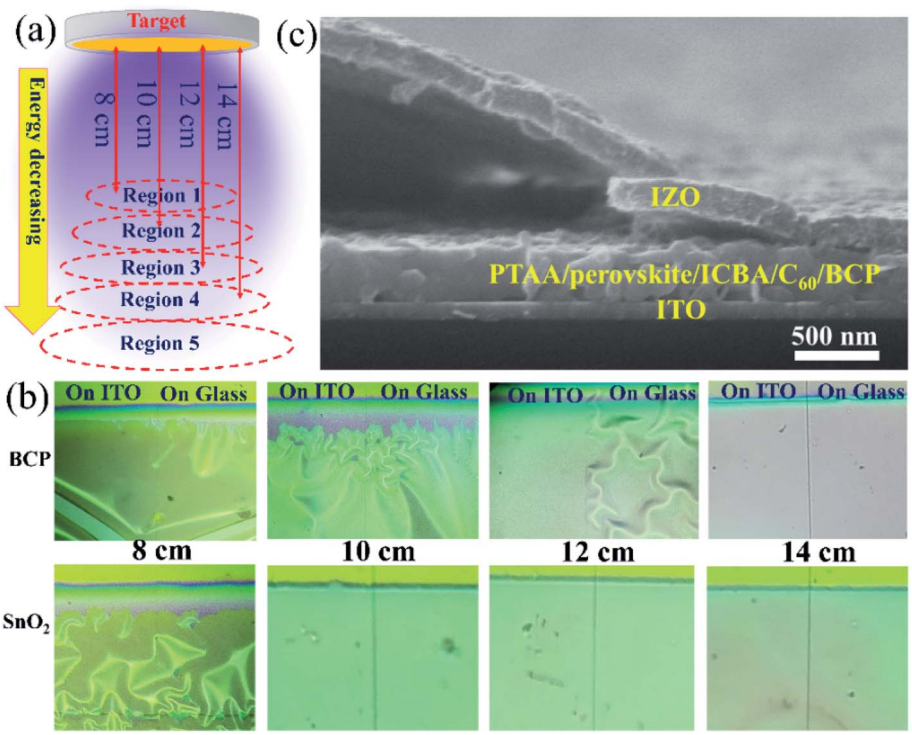

Fig. 1 (a) Schematic diagram of the IZO sputtering process with different target–substrate distances. (b) Different peeling-off results in IZO electrodes after sputtering at target–substrate distances of 8 cm, 10 cm, 12 cm, and 14 cm with BCP or SnO_2 as the buffer layer. (c) Cross-sectional SEM image of a perovskite solar cell with the BCP buffer layer and peeled off IZO electrodes deposited at a target–substrate distance of 10 cm.

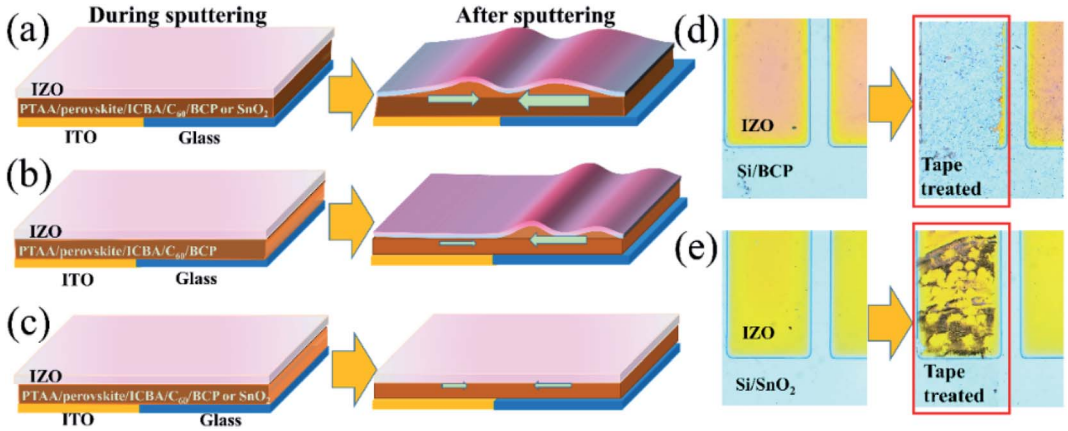

Fig. 2 Schematic diagram of the formation of IZO peeling-off (a) both on the ITO and ITO/glass substrate, and (b) only on the glass side. (c) Schematic diagram of the formation of IZO without peeling-off. (d) IZO fingers on the BCP film before and after being treated with a tape. (e) IZO fingers on the SnO_2 film before and after being treated with a tape.

the sample. It is noted that the sputtered atoms experience collisions with Ar atoms on their path to the substrate, reducing their kinetic energy. Therefore, the temperature of the samples decreases accordingly when they are farther away from the target.

Since the temperature changes with the target–substrate distance, the thermal expansion of underlying films shows the same tendency. As illustrated in Fig. 2a, the different thermal expansion coefficients between layers caused peeling-off of the IZO layer after sputtering during the cooling down process. The thermal expansion coefficients of perovskite and organic layers (3×10^{-5} to 5×10^{-5} K^{-1}) are one order of magnitude higher than those of TCO films and glass substrates (5×10^{-6} to 7×10^{-6} K^{-1}).[28–30] When the samples were placed at a target–substrate distance of 8 cm, the soft perovskite and organic films expanded due to elevated temperature during sputtering; when the solar cells cooled to room temperature after sputtering, the perovskite and organic layers contracted more than the IZO film, which caused large stress in the sputtered IZO film. Specifically, tensile stress formed in perovskite/organic layers and compressive stress formed in the IZO layer. If the stress was large enough (as calculated in the ESI†), it would cause severe peeling-off of the IZO electrode, as shown in Fig. 2a and b. At a target–substrate distance of 14 cm, the lower local temperature resulted in less stress and thus mitigated the peeling-off issue for solar cells with the BCP buffer layer, as shown in Fig. 2c.

2.3 Effects of affinity on IZO peeling-off

We also considered whether the peeling-off of the sputtered IZO electrode was due to the stress caused by the insertion of particles like indium, zinc, or oxygen during sputtering. If this was the case, the peeling-off phenomenon would occur during the sputtering process, rather than during the device cool down process after sputtering, which is opposite to the experimental observation. Moreover, we found that the substrate property also affected the peeling-off location. The substrates we used to make the devices were glass substrates with only half of the area coated with the ITO bottom electrode. When we sputtered the IZO top electrode for BCP-devices at a target–substrate distance of 12 cm, the peeling-off phenomenon of the IZO electrode only occurred at locations without the ITO bottom electrode, as shown in Fig. 1b and S1c.† If the stress induced by insertion of sputtered particles dominated the peeling-off phenomenon, there would be no difference of stress and peeling-off phenomenon in locations with and without the ITO bottom electrode. Therefore, we believe this difference is due to different stress release on different substrates during the cooling down process. In our previous study,[31] we found that the perovskite film coated on a glass side generally showed less strain than the perovskite film coated on ITO/glass slide, which was ascribed to the different bonding strength between the perovskites and substrates due to different roughnesses of ITO and glass. Less affinity or bonding of perovskites to the smooth and nonwetting glass substrates allows the perovskite films on glass release strain much easier than on rough ITO. For the same reason, when the temperature cooled down after sputtering, the perovskite film on glass could have larger contraction than the film on ITO substrates, which created larger stress between the perovskite film and sputtered IZO electrode at the location of bare glass and caused peeling-off, as shown in Fig. 2b.

Since no IZO peeling-off was observed in solar cells based on the SnO_2 buffer layer when IZO was deposited at a target–substrate distance of 10 cm or longer, we speculated that better affinity between SnO_2 with adjacent layers was formed. This is because SnO_2 and IZO are both metal oxides, which will benefit formation of strong bonding between them. Since BCP is an organic molecule, the contact between IZO and BCP is based on van der Waals forces. To verify this, we deposited IZO fingers onto BCP and SnO_2 films on silicon substrates and then tried to tear IZO fingers with tape. Fig. 2d and e show the results of tearing IZO fingers on BCP and SnO_2 films. It was found that the IZO on BCP can be peeled off easily while IZO on SnO_2 was very

firm, which revealed the better affinity between IZO and SnO_2 than that between IZO and BCP. The cross-sectional SEM image of the perovskite solar cell with the SnO_2 buffer layer in Fig. S2† also shows good contact between SnO_2 and IZO layers.

We also studied whether using ALD-SnO_2 can ultimately solve the IZO peeling-off issue by reducing the substrate temperature to an unpractically low value of −5 °C. We found that IZO still peeled off in the SnO_2 samples when the target–substrate distance was 10 cm, as shown in Fig. S3.† No change was observed for the samples when the target–substrate distance was 12 cm or 14 cm. This indicates that an appropriately large target–substrate distance is still needed for SnO_2-devices.

2.4 Influences of sputter induced molecular level damage in BCP

Despite that a large target–substrate distance could generate less stress in the sputtered IZO to avoid the peeling-off issue of the TCO electrode itself, sputtering of IZO could still damage other layers. Perovskite, fullerene, and BCP in the perovskite sub-cells are all soft materials that have either low cohesive energy between the atoms or low bond dissociation energy between the molecules.[16,32] The bombardment of them by high-energy particles might cause atomic or molecular level damage which will reduce their electronic properties. In order to evaluate the influence of sputter damage on electronic properties, we fabricated perovskite solar cells with the structure of ITO/PTAA/perovskite/ICBA/C_{60}/BCP/IZO/Cu by sputtering a 10 nm-thick IZO electrode at a target–substrate distance of 14 cm and then thermally evaporating 80 nm-thick Cu, as shown in Fig. 3a. In this design, the thermally evaporated Cu electrode enhanced the conductivity of the IZO electrode, where the thin IZO electrode was introduced to evaluate the sputter damage. Fig. 3b shows that the IZO/Cu-device exhibited a very low fill factor (FF) and an obvious S-shape in the *J–V* curve, while the control device that only had thermally evaporated Cu electrode performed much well. This indicates that the sputtering process still caused damage to the other layers.[15] If the Cu electrode was also deposited by sputtering rather than by thermal evaporation, a similar *J–V* curve with a low FF and S-shape was also found (Fig. S4†), which further proves that the worse device performance was caused by sputter damage, rather than the new interfaces introduced by IZO. This suggests that even though a larger sputtering distance can avoid the stress issue, it cannot completely eliminate the sputter caused molecular level damage in the BCP buffer layer.

2.5 MD simulation on molecular level damage in BCP

In order to reveal how BCP was damaged, we performed MD simulations on the collision process between sputtered indium atoms and BCP molecules. The indium atom was selected because it has the highest mass compared to zinc, oxygen, and argon atoms. According to the law of conservation of momentum, indium atoms will loss less kinetic energy per collision with, *e.g.*, Ar atoms than other sputtered atoms, and will thus arrive at the substrate with the most energy. The energies of

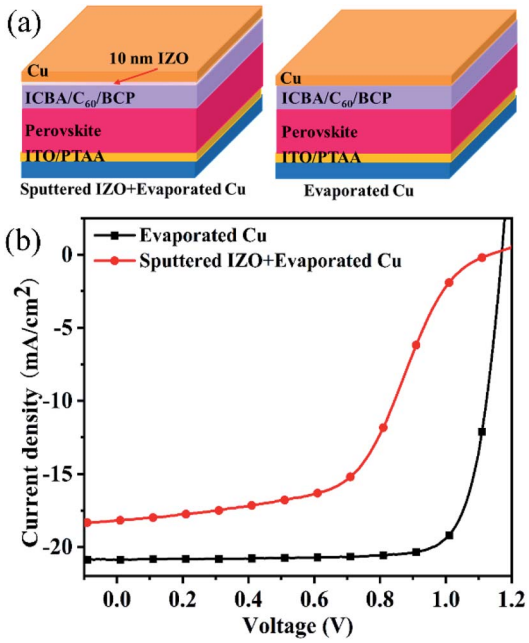

Fig. 3 (a) Schematics of perovskite solar cells with and without a 10 nm-thick IZO film under the Cu electrode. (b) *J–V* characteristics of the perovskite solar cells with Cu and IZO/Cu electrodes.

indium atoms in the range of 1 eV to 10 eV were simulated. We also varied the incidence of the indium atoms to hit different atoms in BCP, and we found that the C–C bond connecting the methyl group was the most easily broken. Therefore, the damage was most likely to occur at the C–C bond in BCP during sputtering, and we focused our simulation at this position. Fig. 4a–c shows simulated collision processes with three different indium energies near the damage threshold. For indium atoms with an energy of 5 eV, the methyl group did not change its position and the distance of adjacent two carbon atoms remained the same after collision (Fig. 4a). For indium atoms with energi of 6 eV and

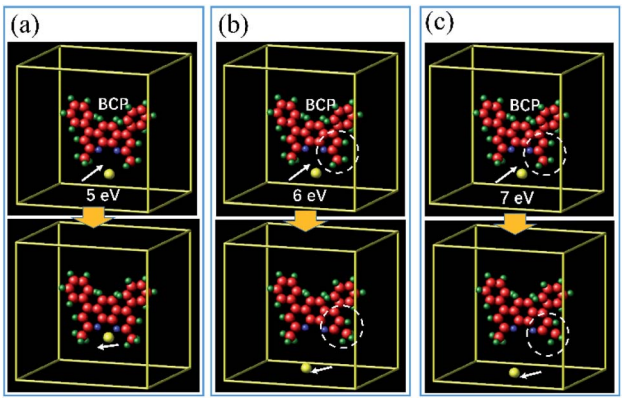

Fig. 4 MD simulations of collisions between sputtered indium atoms and BCP molecules. The incident energy of the indium atoms is set to (a) 5 eV, (b) 6 eV, and (c) 7 eV. The first row shows the system before collision; the second row shows the system after collision. The circles in (b) and (c) denote differences in the position and distance of atoms, which can illustrate the damage in BCP.

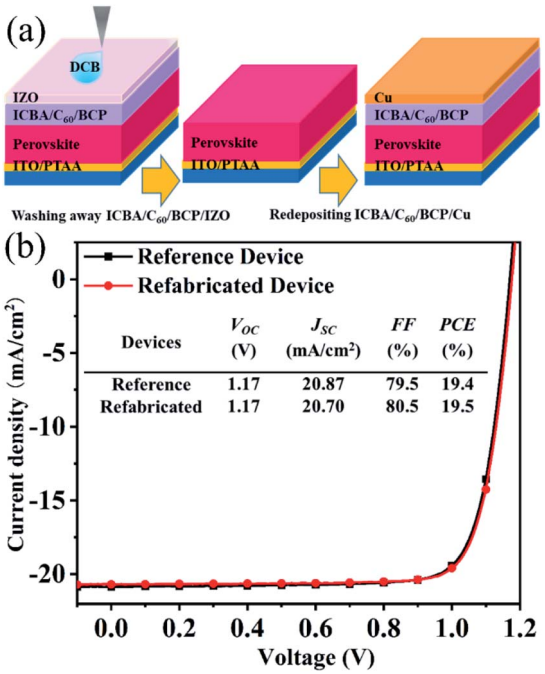

Fig. 5 (a) Procedure for refabricating a perovskite solar cell by replacing ICBA/C_{60}/BCP/IZO with new layers of ICBA/C_{60}/BCP/Cu. (b) *J–V* characteristics of the perovskite solar cell after refabrication, compared to a control device with an original Cu electrode.

7 eV, the methyl group was bombarded away from its original position and the distance of adjacent two carbon atoms was changed (Fig. 4b and c). This reveals that the C–C bond in BCP can be broken by indium atoms with an energy of 6 eV and higher. This energy threshold indicates the reason why sputter damage could occur in BCP but not in SnO_2. This is because the Sn–O bond energy in SnO_2 films is about 528 kJ mol^{-1} (5.47 eV),[33] which is much higher than the C–C bond energy (3.59 eV) in BCP molecules. This means that it requires a higher energy for sputtered atoms to break down SnO_2.

2.6 Investigation on damage of underlying layers

Since the device efficiency reduction can come from damage of any layer in the perovskite solar cells, we studied whether the sputter damage penetrated into other layers underneath BCP for solar cells with BCP or SnO_2 buffer layers. We fabricated a perovskite solar cell with sputtered IZO electrodes, and then we washed off the ICBA/C_{60}/BCP/IZO layers with 1,2-dichlorobenzene (DCB), as shown in Fig. 5a. We next deposited ICBA/C_{60}/BCP/Cu on the perovskite again. Fig. 5b shows the *J–V* results of the re-fabricated device and the reference device with evaporated Cu electrodes on BCP directly. The original perovskite solar cell with the sputtered IZO electrode here has an S-curve similar to the *J–V* curve of the solar cell with IZO/Cu in Fig. 3b. However, we can see that the re-fabricated device does not show any performance degradation compared to the reference device,

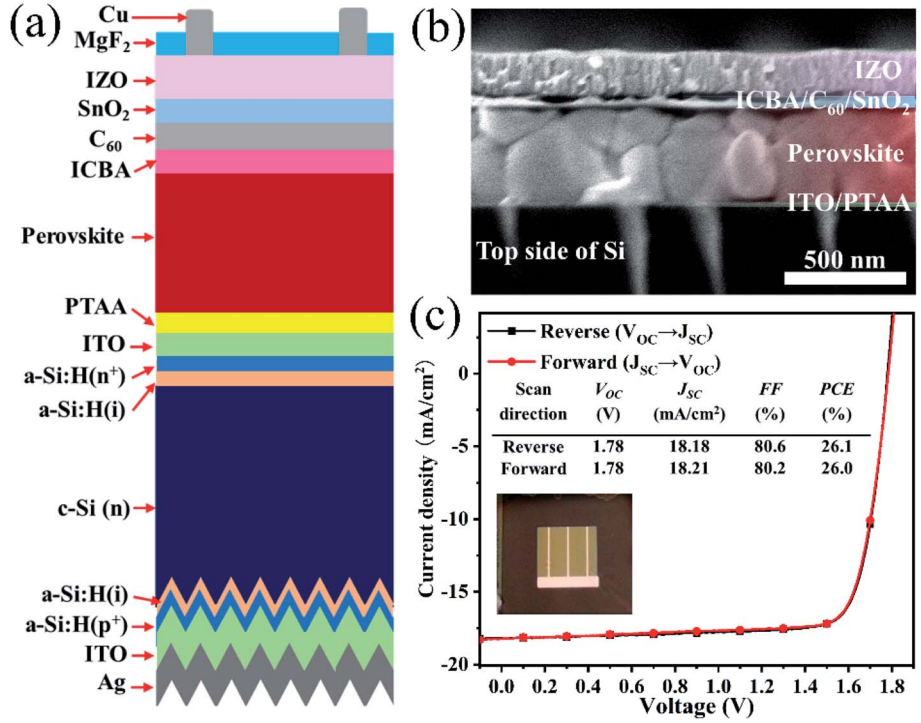

Fig. 6 (a) Schematic of the perovskite/silicon tandem solar cell with the SnO_2 buffer layer. (b) Cross-sectional SEM image of the perovskite top sub-cell of the tandem solar cell. (c) *J–V* characteristics of the perovskite/silicon tandem solar cell under forward and reverse scans. Inset in (c): image of the perovskite/silicon monolithic tandem solar cell.

which has the same *J–V* curve of the solar cell with evaporated Cu in Fig. 3b. This reveals that the sputtering process did not damage the underlying perovskite layer. For further verification, we performed MD simulations on collisions between indium atoms and C_{60} molecules with different atom energies. Fig. S5† shows that bond rupture in the C_{60} molecule happens only when the energy of the sputtered indium exceeds 200 eV, which is much higher than the initial energy of sputtered atoms from the target. For indium atoms with energy lower than 200 eV, no obvious changes were found in the C_{60} structure. Besides, the indium atoms were reflected back by the carbon atoms. Therefore, it is unlikely that the sputtered atoms can cause damage to the layers underneath the C_{60} layer and we only need to consider the sputter damage issues in the BCP layer.

2.7 Achieving efficient perovskite/silicon tandem solar cell

Since the substrate–target distance of 14 cm is still not large enough to avoid the damage of BCP by high energy particles during the sputtering process, we attempted to further increase the substrate–target distance. However, both the conductivity and transmittance of IZO films become worse when the target–substrate distance was increased to beyond 14 cm, as shown in Fig. S6.† This is because sputtered atoms with too low energy generally result in porous and rough morphology of the IZO film.[34,35] SnO_2 is an excellent buffer layer to allow a wide range of target–substrate distances to resist the sputter damage as well as to tolerate the sputter induced stress, which enable fabrication of efficient semi-transparent perovskite solar cells and tandem solar cells.

We fabricated a complete perovskite/silicon tandem solar cell with the SnO_2 buffer layer and IZO electrode deposited at a target–substrate distance of 12 cm to check the beneficial effects of elimination of sputter damage and the peeling-off issue. Fig. 6a shows the structure of the tandem device. The corresponding cross-sectional SEM image of the perovskite sub-cell in Fig. 6b also shows good contact between each layers without the peeling-off issue. No peeling-off of the IZO electrode was observed after the tandem device cooled to −5 °C to enlarge the residual stress, which indicates strong adhesion between the IZO electrode and underlying layers. Thanks both to the sputter protection provided by SnO_2 and the optimized IZO sputtering process, the tandem solar cell reached a PCE of 26.0% (Fig. 6c). There was no obvious PCE degradation for the un-encapsulated tandem device under illumination at a maximum power point at ∼55 °C in air for 120 min (Fig. S7†). The external quantum efficiency (EQE) result of the tandem device shows that the current of two sub-cells matched well (Fig. S8†). The absence of hysteresis and high FF indicate that the charge recombination and interfacial barrier introduced by sputter damage and stress have been suppressed due to reduction of sputter damage using the optimized sputtering conditions and SnO_2 buffer layers.

3 Conclusions

In summary, we investigated the sputtering process of IZO electrodes on the perovskite top sub-cell of perovskite/silicon tandem solar cells with focus on the mechanism for peeling-off and sputter damage. The peeling-off of the sputtered IZO electrode was avoided by increasing the target–substrate distance to 14 cm for the BCP buffer layer and 10 cm for the SnO_2 buffer layer, but sputter damage to the BCP buffer layer persisted at these distances. MD simulations showed that energetic sputtered atoms with a kinetic energy greater than 6 eV can break C–C bonds in BCP molecules. It was proved that the buffer layer is the key to address the sputter damage issue, because the sputter damage did not penetrate into the underlying layers. When utilizing SnO_2 as the buffer layer, strong affinity between sputtered IZO and buffer layer was formed and thus the peeling-off issue was suppressed. A high PCE of 26.0% was obtained in a perovskite/silicon tandem solar cell when these strategies were applied. This work demonstrates that the combination of an appropriate target–substrate distance and a robust buffer layer is a solution to suppress the stress in IZO films and avoid the bond rupture in the buffer layer.

Author contributions

J. H., Z. H., B. C., and S. Q. conceived the idea. K. L. conducted sputtering deposition and molecular dynamics simulation. K. L. and B. C. fabricated the wide-bandgap solar cells and perovskite/silicon tandem cells. Z. Y. fabricated the silicon bottom cells. Y. W. fabricated films and conducted the SEM test. Z. H. and X. J. performed the calculations. D. S. and C. L. carried out ALD. Z. W. and Z. W. analysed optical and electrical properties of TCO. K. L., B. C., and J. H. wrote the paper, and all authors reviewed the paper.

Conflicts of interest

There are no conflicts to declare.

Acknowledgements

The information, data, or work presented herein is funded by U.S. Department of Energy's Office of Energy Efficiency and Renewable Energy (EERE) under Solar Energy Technologies Office (SETO) (Agreement Number DE-EE0008749) and by the UNC Research Opportunities Initiative through the Center of Hybrid Materials Enabled Electronic Technology. Prof. K. Liu also acknowledges the support from Youth Innovation Promotion Association, Chinese Academy of Sciences (No. 2020114).

References

1 K. A. Bush, C. D. Bailie, Y. Chen, A. R. Bowring, W. Wang, W. Ma, T. Leijtens, F. Moghadam and M. D. McGehee, *Adv. Mater.*, 2016, **28**, 3937–3943.
2 H. R. Tan, A. Jain, O. Voznyy, X. Z. Lan, F. P. G. de Arquer, J. Z. Fan, R. Quintero-Bermudez, M. J. Yuan, B. Zhang, Y. C. Zhao, F. J. Fan, P. C. Li, L. N. Quan, Y. B. Zhao, Z. H. Lu, Z. Y. Yang, S. Hoogland and E. H. Sargent, *Science*, 2017, **355**, 722–726.

3 G. E. Eperon, T. Leijtens, K. A. Bush, R. Prasanna, T. Green, J. T. W. Wang, D. P. McMeekin, G. Volonakis, R. L. Milot, R. May, A. Palmstrom, D. J. Slotcavage, R. A. Belisle, J. B. Patel, E. S. Parrott, R. J. Sutton, W. Ma, F. Moghadam, B. Conings, A. Babayigit, H. G. Boyen, S. Bent, F. Giustino, L. M. Herz, M. B. Johnston, M. D. McGehee and H. J. Snaith, *Science*, 2016, **354**, 861–865.

4 M. B. Upama, M. A. Mahmud, H. M. Yi, N. K. Elumalai, G. Conibeer, D. Wang, C. Xu and A. Uddin, *Org. Electron.*, 2019, **65**, 401–411.

5 T. Leijtens, K. A. Bush, R. Prasanna and M. D. McGehee, *Nat. Energy*, 2018, **3**, 828–838.

6 Y. G. Rong, Y. Hu, A. Y. Mei, H. R. Tan, M. I. Saidaminov, S. I. Seok, M. D. McGehee, E. H. Sargent and H. W. Han, *Science*, 2018, **361**, eaat8235.

7 Z. S. Yu, M. Leilaeioun and Z. Holman, *Nat. Energy*, 2016, **1**, 16137.

8 Z. S. J. Yu, J. V. Carpenter and Z. C. Holman, *Nat. Energy*, 2018, **3**, 747–753.

9 L. K. Zheng, J. L. Wang, Y. M. Xuan, M. Y. Yan, X. X. Yu, Y. Peng and Y. B. Cheng, *J. Mater. Chem. A*, 2019, **7**, 26479–26489.

10 K. A. Bush, A. F. Palmstrom, Z. S. J. Yu, M. Boccard, R. Cheacharoen, J. P. Mailoa, D. P. McMeekin, R. L. Z. Hoye, C. D. Bailie, T. Leijtens, I. M. Peters, M. C. Minichetti, N. Rolston, R. Prasanna, S. Sofia, D. Harwood, W. Ma, F. Moghadam, H. J. Snaith, T. Buonassisi, Z. C. Holman, S. F. Bent and M. D. McGehee, *Nat. Energy*, 2017, **2**, 17009.

11 F. Sahli, J. Werner, B. A. Kamino, M. Brauninger, R. Monnard, B. Paviet-Salomon, L. Barraud, L. Ding, J. J. D. Leon, D. Sacchetto, G. Cattaneo, M. Despeisse, M. Boccard, S. Nicolay, Q. Jeangros, B. Niesen and C. Ballif, *Nat. Mater.*, 2018, **17**, 820–826.

12 M. Jost, E. Kohnen, A. B. Morales-Vilches, B. Lipovsek, K. Jager, B. Macco, A. Al-Ashouri, J. Krc, L. Korte, B. Rech, R. Schlatmann, M. Topic, B. Stannowski and S. Albrecht, *Energy Environ. Sci.*, 2018, **11**, 3511–3523.

13 B. Chen, Z. Yu, K. Liu, X. Zheng, Y. Liu, J. Shi, D. Spronk, P. N. Rudd, Z. Holman and J. Huang, *Joule*, 2019, **3**, 177–190.

14 T. Minami, *Thin Solid Films*, 2008, **516**, 5822–5828.

15 H. Kanda, A. Uzum, A. K. Baranwal, T. A. N. Peiris, T. Umeyama, H. Imahori, H. Segawa, T. Miyasaka and S. Ito, *J. Phys. Chem. C*, 2016, **120**, 28441–28447.

16 H. Lei, M. H. Wang, Y. Hoshi, T. Uchida, S. Kobayashi and Y. Sawada, *Appl. Surf. Sci.*, 2013, **285**, 389–394.

17 X. P. Zheng, Y. Hou, C. X. Bao, J. Yin, F. L. Yuan, Z. R. Huang, K. P. Song, J. K. Liu, J. Troughton, N. Gasparini, C. Zhou, Y. B. Lin, D. J. Xue, B. Chen, A. K. Johnston, N. Wei, M. N. Hedhili, M. Y. Wei, A. Y. Alsalloum, P. Maity, B. Turedi, C. Yang, D. Baran, T. D. Anthopoulos, Y. Han, Z. H. Lu, O. F. Mohammed, F. Gao, E. H. Sargent and O. M. Bakr, *Nat. Energy*, 2020, **5**, 131–140.

18 D. Y. Luo, W. Q. Yang, Z. P. Wang, A. Sadhanala, Q. Hu, R. Su, R. Shivanna, G. F. Trindade, J. F. Watts, Z. J. Xu, T. H. Liu, K. Chen, F. J. Ye, P. Wu, L. C. Zhao, J. Wu, Y. G. Tu, Y. F. Zhang, X. Y. Yang, W. Zhang, R. H. Friend, Q. H. Gong, H. J. Snaith and R. Zhu, *Science*, 2018, **360**, 1442–1446.

19 J. Y. Jeng, Y. F. Chiang, M. H. Lee, S. R. Peng, T. F. Guo, P. Chen and T. C. Wen, *Adv. Mater.*, 2013, **25**, 3727–3732.

20 N. Shibayama, H. Kanda, T. W. Kim, H. Segawa and S. Ito, *APL Mater.*, 2019, **7**, 031117.

21 R. Xia, Y. B. Xu, B. B. Chen, H. Kanda, M. Franckevicius, R. Gegevicius, S. B. Wang, Y. F. Chen, D. M. Chen, J. N. Ding, N. Y. Yuan, Y. Zhao, C. Roldan-Carmona, X. D. Zhang, P. J. Dyson and M. K. Nazeeruddin, *J. Mater. Chem. A*, 2021, **9**, 21939–21947.

22 A. Al-Ashouri, E. Kohnen, B. Li, A. Magomedov, H. Hempel, P. Caprioglio, J. A. Marquez, A. B. M. Vilches, E. Kasparavicius, J. A. Smith, N. Phung, D. Menzel, M. Grischek, L. Kegelmann, D. Skroblin, C. Gollwitzer, T. Malinauskas, M. Jost, G. Matic, B. Rech, R. Schlatmann, M. Topic, L. Korte, A. Abate, B. Stannowski, D. Neher, M. Stolterfoht, T. Unold, V. Getautis and S. Albrecht, *Science*, 2020, **370**, 1300–1309.

23 Y. Hou, E. Aydin, M. De Bastiani, C. Xiao, F. H. Isikgor, D.-J. Xue, B. Chen, H. Chen, B. Bahrami, A. H. Chowdhury, A. Johnston, S.-W. Baek, Z. Huang, M. Wei, Y. Dong, J. Troughton, R. Jalmood, A. J. Mirabelli, T. G. Allen, E. Van Kerschaver, M. I. Saidaminov, D. Baran, Q. Qiao, K. Zhu, S. De Wolf and E. H. Sargent, *Science*, 2020, **367**, 1135–1140.

24 J. Xu, C. C. Boyd, Z. J. Yu, A. F. Palmstrom, D. J. Witter, B. W. Larson, R. M. France, J. Werner, S. P. Harvey, E. J. Wolf, W. Weigand, S. Manzoor, M. F. A. M. van Hest, J. J. Berry, J. M. Luther, Z. C. Holman and M. D. McGehee, *Science*, 2020, **367**, 1097–1104.

25 H. R. Liu, Z. L. Chen, H. B. Wang, F. H. Ye, J. J. Ma, X. L. Zheng, P. B. Gui, L. B. Xiong, J. Wen and G. J. Fang, *J. Mater. Chem. A*, 2019, **7**, 10636–10643.

26 T. Motohiro and Y. Taga, *Thin Solid Films*, 1984, **112**, 161–173.

27 P. F. Carcia, R. S. McLean, M. H. Reilly, Z. G. Li, L. J. Pillione and R. F. Messier, *J. Vac. Sci. Technol., A*, 2003, **21**, 745–751.

28 Y. Rakita, S. R. Cohen, N. K. Kedem, G. Hodes and D. Cahen, *MRS Commun.*, 2015, **5**, 623–629.

29 M. N. Saleh and G. Lubineau, *Sol. Energy Mater. Sol. Cells*, 2014, **130**, 199–207.

30 A. T. Pugachev, N. P. Churakova, N. I. Gorbenko, K. Saadli and E. S. Syrkin, *J. Exp. Theor. Phys.*, 1998, **87**, 1014–1018.

31 J. J. Zhao, Y. H. Deng, H. T. Wei, X. P. Zheng, Z. H. Yu, Y. C. Shao, J. E. Shield and J. S. Huang, *Sci. Adv.*, 2017, **3**, eaao5616.

32 E. Salonen, K. Nordlund, J. Keinonen and C. H. Wu, *Europhys. Lett.*, 2000, **52**, 504–510.

33 M. Fondell, M. Gorgoi, M. Boman and A. Lindblad, *J. Electron Spectrosc.*, 2014, **195**, 195–199.

34 J. A. Thornton, *J. Vac. Sci. Technol.*, 1974, **11**, 666–670.

35 J. H. E. Cartwright, B. Escribano, O. Piro, C. I. Sainz-Diaz, P. A. Sanchez and T. Sintes, *AIP Conf. Proc.*, 2008, **982**, 696–701.